Nanofabrication of flexible thin-film bioelectronics for long-term stable neural signal recording

By

Ariel J. Lee

B.S., Korea Advanced Institute of Science and Technology (2021)

Submitted to the Department of Electrical Engineering and Computer Science in Partial Fulfillment of the Requirements for the Degree of

Master of Science

at the

MASSACHUSETTS INSTITUTE OF TECHNOLOGY

FEBRUARY 2024

Authored by: Ariel J. Lee
Department of Electrical Engineering and Computer Science
January 26, 2024

Certified by: Xiao Wang
Assistant Professor of Chemistry
Thesis Supervisor

Certified by: Jia Liu
Assistant Professor of Bioengineering, Harvard University
Thesis Supervisor

Accepted by: Leslie A. Kolodziejski
Professor of Electrical Engineering and Computer Science Chair,
Department Committee on Graduate Students

Nanofabrication of flexible thin-film bioelectronics for long-term stable neural signal recording

By

Ariel J. Lee

Submitted to the Department of Electrical Engineering and Computer Science
in Partial Fulfillment of the Requirements for the Degree of

Master of Science

ABSTRACT

Establishing a long-term stable and effective interface for brain is a significant milestone for all neural implants. Recent studies have demonstrated that tissue-level soft and flexible materials and devices can provide such stability for neural implants. Therefore, engineering suitable materials and developing fabrication methods for soft and flexible thin-film electric probes to further exploit their potential are essential to advancing the field. This thesis demonstrates the comprehensive methods required for developing electrical recording devices and for analyzing the acquired neural data. It presents the design, fabrication, and *in vivo* implantation of flexible thin-film electronic devices. The materials and fabrication processes are engineered to create structures that can more closely mimic the mechanical properties of brain tissue, in contrast to traditional stiff neural probes. The device designs in this work feature serpentine-shaped ribbons for stretchability and tetrode-like electrode configuration to enable the measurement of single-unit neural activities.

Thesis Supervisor: Xiao Wang
Assistant Professor of Chemistry

Jia Liu
Assistant Professor of Bioengineering, Harvard University

Acknowledgements

Firstly, I would like to thank my advisors, Professor Jia Liu and Professor Xiao Wang, for their unwavering support, patience, and belief in my ability to explore a new research field. Their guidance has been invaluable, providing me with the opportunity to learn and delve into new horizons. I greatly look forward to continuing this research journey under their mentorship.

A sincere thank you goes to my group members, especially to Hao Sheng, Xinyi Lin, Xinhe Zhang, Ren Liu, and Jaeyong Lee, whose diverse expertise has enriched my understanding across various domains. The completion of this research owes much to their collaborative efforts and support.

I am deeply indebted to my mentors from my previous research experiences, Professors Yongkeun Park, Woonggyu Jung, and Gary Tearney. Their support made it possible for me to conduct research at MIT and Harvard, adding invaluable insights to my academic journey. Meeting and learning from them has been an extraordinary and fortunate chapter in my academic pursuits.

Special recognition is due to my family for their limitless love and support. Thank you, Mom and Dad, for your belief in me and encouragement to pursue my true aspirations and find happiness, which have played a pivotal role in shaping the person I am today. To my brother, Daniel, thank you for your love and engaging in enjoyable discussions on random yet intriguing scientific problems. Lastly, to my husband, Minchan, my recent addition to the family, thank you so much for all your love and for being my best friend. I am profoundly thankful to have you by my side in this journey, and in all the ones to come.

Table of Contents

List of Figures

Chapter 1

1. Introduction

Brain-machine interface (BMI), or brain-computer interface (BCI), establishes a direct line of communication between the brain and external devices[1]. Through BMI, information can be exchanged in both directions, providing access to neural signals and enabling the brain to control machines. This is very exciting because it has the potential to revolutionize how humans interact with technology, with multiple applications in healthcare, assistive technology, entertainment, or even the enhancement of human capabilities[2–4].

Although a BMI system is composed of numerous components, one of the most essential and necessary components is the probe that collects and sends neural signals. Neurons generate electrical impulses, or action potentials, which occur due to rapid changes in the electrical potential across the neuronal cell membrane. One popular method for collecting these changes is to insert electrodes inside the brain, near the neurons, and record the induced electric signals transmitted through the electronic device. There also exist less invasive methods for recording neural signals such as electroencephalogram (EEG)[5,6] and electrocorticography (ECoG)[7,8]. However, these methods are out of scope of this thesis since they can only acquire low spatio-temporal resolution signals.

This thesis demonstrates an experimental study to fabricate thin-film brain probes capable of establishing stable signal recordings from neurons *in vivo*. Suitable materials and designs are engineered to fabricate a flexible and stretchable structure that better matches the mechanical properties of brain tissue while

ensuring the electrical characteristics meet the requirements for acquiring low signal-to-noise ratio signals from the neurons.

1.1 Flexible Electronics for Brain-machine Interface

A safe and effective brain implant should be able to establish and maintain a stable and effective connection with the brain. However, this is very challenging for traditional brain implantable probes for several reasons. Firstly, the materials used for the probes are often not entirely biocompatible or may release toxic molecules over time due to corrosion[9,10]. If ions can penetrate through the encapsulation material, which is supposed to separate the metal component of the probe from the saline-rich biological tissue, the signal degrades over time. Additionally, most traditional probes exhibit significant mechanical and geometrical mismatch with brain tissue. This allows drift of the probe due to micromotions, which can chronically damage the tissue and trigger immune responses. Maintaining consistent quality of signal over time becomes difficult as the probe's position changes physically, and scar sheath develops around the probe. Therefore, it would be highly beneficial if brain probes could be made as flexible and soft as the brain tissue, with encapsulation materials that are biocompatible and provide effective ionic passivation over time.

1.2 Thin-film Electronics for Neural Interface

Traditional neural probes that are not flexible or soft are typically fabricated using two main methods. Firstly, chemically etching silicon produces an array of spikes, which are then metalized and coated to reduce the electrodes' impedance values[11]. Alternatively, insulating and conductive materials are patterned layer-by-layer on a silicon wafer using microfabrication techniques such as chemical vapor deposition, wet/dry etching, or lift-off processes[12]. These devices commonly employ materials with a Young's modulus approximately 10^7 to 10^8 times higher than that of brain tissues[13].

Researchers have been exploring the use of materials with lower Young's modulus and reduced film thickness to decrease bending stiffness[14]. Various morphologies of the probes have been developed, such as thin-film parallel probes, injectable mesh and threads. For example, Chung et al. have developed a polymer-based high-density polyimide electrode array[15]. They have decreased the thickness to 14 μm despite employing four polyimide (PI) layers and three conductive layers. Luan et al. have fabricated nanoelectronic thread electrodes using SU-8 as the encapsulation material and gold as conductive layer, achieving a total thickness of 1 μm[16].

1.3 Long-term Stable Brain Recordings

By employing such flexible and soft neural probes, researchers have successfully measured electrical signals from live animals for several months, and in some cases, even more than a year, with remarkably stable recordings. For instance, Fu et al. have developed a thin-film flexible mesh-like electrode using SU-8 and gold each as encapsulation and conductive layers, respectively. This electrode was able to record stable *in vivo* neuronal signals for at least 8 months[17]. The researchers tracked neural activities at the single-neuron level and identified neural firing dynamics alterations related to aging. Additionally, Zhao et al. have demonstrated that their flexible probe could track the same neuron's signal throughout the entire adult life of mice. This research clearly showcases the capability of thin-film electronics to stably record neural signals for extended periods of time[18].

Chapter 2

2. Design of Thin-film Flexible Electronics

As briefly discussed in the previous chapter, the fabrication of thin-film flexible electronics is often accomplished using micro-nano fabrication techniques, wherein each layer is fabricated sequentially. During these processes, each step has its own unique materials and/or morphological limitations due to the procedural characteristics. Therefore, it is critical to design each layer of the device with the limitations and capabilities of each fabrication process in mind. The design choices can be broadly divided into two categories: material and probe morphology.

2.1 Materials Selection

As for considering which materials to choose for each component of the device, there are three different components to most of the electronic neural probes: encapsulation, interconnect, and recording site. Especially for chronic implants, the encapsulation material's low ionic conductivity level over time and the intrinsic biocompatibility of the materials are crucial factors. Polymers such as epoxy-based polymer SU-8 and PI have been widely used as encapsulation materials due to their biostability of the passivation and biocompatibility[19]. However, they lack flexibility or softness compared to other elastomers such as polydimethylsiloxane (PDMS) or styrene−ethylene−butylene−styrenecopolymer (SEBS). The mechanical property is also a crucial factor to consider when building flexible devices, but the impedance of PDMS or SEBS layers deteriorate rapidly under physiological environments[20]. In addition, both materials are not

directly patternable using photolithography and thus necessitates additional fabrication steps such as mold or mask fabrication.

Recently, perfluoropolyether (PFPE)-based elastomers that can be patterned using photolithography have demonstrated stable high electrochemical impedance in saline environments and have 10^4 order softer mechanical properties compared to SU-8 or PI[21]. For our thin-film electronics, materials such as SU-8 and PFPE-based elastomers can be utilized as the encapsulation layer, patterned into cellular-level scale designs using photolithography. SU-8 is a negative photoresist, thus the region exposed to the ultraviolet (UV) light becomes cross-linked and is left on the wafer after developing the layer. SU-8 is spin-coated on a silicon dioxide wafer to a desired thickness and baked, exposed with UV light, and developed to be patterned and hard-baked to further stabilize the polymer layer. There are various types of SU-8, and for our device, S2000.5 or S2002 can be used to achieve clean patterning result and desired thickness of less than 1 μm to 2 μm.

PFPE-based elastomers are highly soft and stable polymer that has much lower elastic modulus than PDMS, achieving much similar softness to brain tissues more than SU-8 or PI. There are multiple different types of PFPE-based elastomers but for dimethacrylate-modified PFPE (PFPE-DMA) was found to have high electrochemical impedance, similar to SU-8. PFPE-DMA can be photo-crosslinked[22], and its monomer and solvent need to be synthesized in the lab and the mechanical characteristics such as stretchability of the crosslinked polymer are altered based on the monomer's molecular weight.

While SU-8 is less stretchable or soft compared to brain tissue or PFPE-DMA, it remains suitable for designing devices not requiring prolonged implantation time or stability. Morphological designs can make the device effectively flexible enough for short-term neural signal analysis. Fabrication processes of SU-8 are well-established, and the resulting polymer has higher elastic modulus, which makes it easier to fabricate and handle than PFPE-DMA. In addition, PFPE-DMA film has very stable bonds, which is good for the application, but it makes surface modification more difficult to have better compatibility with a different layer. The UV exposure-induced crosslinking occurs in an oxygen-free N_2 environment, which

complicates the fabrication. Thus, in this thesis, to make the fabrication process simpler and keep the major focus in the morphology design, SU-8 is used as the passivation material, and instead, the device will be designed as a thin-film with mesh structure will allow the device to be effectively flexible and deformable when implanted.

However, since PFPE-based elastomers' mechanical property is evidently a great advantage, various studies are utilizing PFPE-based polymers for multi-layer devices or long-term stable recording applications. For this study, the longest implantation period is less than a month, thus SU-8 was selected as the passivation material for this application.

For interconnects, choosing materials with high conductivity is important. The interconnects' cross-section area is inevitably very small, because the width will be in the order of several micrometers and the thickness less than a micrometer. On the other hand, the length is much longer, up to several centimeters, thus larger in the order of 10^{10}. Thus, in order to achieve effectively high conductance for the interconnects, it is crucial to choose high conductivity-materials.

$$conductance = conductivity \frac{cross\ section\ area}{length}$$

By choosing inherently flexible and soft materials, it is much easier to build more flexible and softer electronic devices. This applies to not only the encapsulation materials but also for the interconnects. Thus, to make electrodes soft, researchers have used liquid metal such as eutectic gallium indium or conductive polymers for interconnects[23]. Although new materials and fabrication methods are being developed for these approaches, conductive polymers yet have incomparably lower conductivity compared to metals and liquid metals are difficult to fabricate with high enough resolution and stability for our single-neuron level brain signal recording electronics device.

Metals are highly conductive materials that can be fabricated into patterns with nano-size resolutions, but other factors such as biocompatibility and mechanical properties must also be considered. Metals such as gold, platinum, iridium and tungsten are relatively safe, whereas silver, iron and copper are toxic[24]. Gold

was selected as the interconnect material for its good electrical conductivity, biocompatibility, and mechanical properties when physically vapor deposited. Gold ranks third in electrical conductivity at 4.5×10^7 S/m, following silver and copper. It does not corrode, remains stable in biological environments, and has a Young's modulus of 79 GPa, which is lower than that of copper or silver.

The recording sites, or electrodes, are exposed and in direct contact with tissue. Therefore, biocompatibility and stability are even more crucial for electrodes than for interconnects. Recording sites must exhibit low interfacial impedance, which is essential for accurate and reliable neural signal recording. One method to achieve low interfacial impedance is by increasing the surface area of the recording sites. Electrochemically depositing conductive polymers such as platinum-black or poly (3, 4-ethylenedioxythiophene):poly(styrene sulfonate) (PEDOT:PSS) are widely used for this purpose.

2.2 Morphology Design

For the morphology of the probes, research has shown that reducing the size of the electrodes to the order of a neuronal body's size effectively forms a stable interface with brain tissue [25]. The average soma size is around 20 μm for mice[26], allowing electrodes to be designed to have a size of around 20 μm. This size range not only decreases the mechanical mismatch between the device and the tissue but also enhances sensitivity for single-unit sensing. Also, metals with much higher Young's modulus than tissues can have their bending stiffness reduced by decreasing the width and thickness of the electrode. By designing the metal interconnect layers to be thinner and narrower, the device and tissue experiences less mechanical mismatch resulting in reduced immune response in brain tissue. Gold conductive interconnects are patterned into thin cables with a thickness of 70 nm to further reduce the bending stiffness. In addition to this, incorporating thicker and softer encapsulation material to surround the relatively less flexible and harder interconnect material allows the surrounding tissue to experience less strain during micro-motion, leading to less local irritation and inflammation.

To fabricate such flexible and durable probes, it is important to consider the biocompatibility of materials, electrical properties, and effective Young's modulus of the multi-layer electronics collectively, while also determining appropriate nanolithography processes.

In addition to designing a flexible probe, a serpentine-shaped interconnect design is incorporated in this thesis's device designs enhance the probe's stretchability. The serpentine-shaped ribbon design keeps the intrinsic strain lower compared to other designs when the device is stretched[27]. Thus, this structure allows the device to stretch with lower risk of breakage, ensuring continuous and stable signal recording capability. Based on these a few design factors for thin-film electronics to be flexible and stretchable, two types of thin-film neural signal recording probe were designed.

Fig. 1a shows the first design of the thin-film flexible device with serpentine-shaped interconnects. For this device, the electrode faces down, opened towards the wafer. The electrodes are positioned into a line, having distance from the closest other electrode of around 90 μm. Each electrode has diameter of 50 μm, and there are 16 channels in each device. The gold (Au) interconnect is sandwiched in between two SU-8 passivation layers. Fig. 1b shows the design of each layer composing the thin-film probe. The top SU-8 layer leaves out some part of the Au input/output (I/O) pads for external cable connection. Fig. 1c shows each layer design and the actual photographs after each fabrication steps. The fabrication method will be explained in detail in the next chapter. Fig. 1d is a photograph of a finished device for this device design, showing the arrangement of the electrodes and serpentine-shaped ribbons. In Fig. 1e, the Au interconnects are well-covered with the SU-8 passivation layers and in Fig. 1f, the top SU-8 layer is covering the electrode from the top, and the bottom SU-8 only covering up to the Au interconnect, not the Pt electrode. This inverted type of device requires a different technique for fabrication, and this is also explained in the next chapter.

For the second design, the I/O pads and the overall design of the device is similar to the first design, as can be seen in Fig. 2a. However, for this device, the entire probe has 30 electrodes with diameter of 20 μm. 6 electrodes together form a tetrode-like geometry, and therefore there are 5 tetrode-like electrode groups. The center-to-center distance between the closest electrodes in each tetrode-like electrode groups is 30 μm.

This allows for simultaneous recording of signals from a single neuron in different electrodes from a same tetrode-like group. By having a tetrode-like electrode groups, it is much easier to identify the real neural signal from noises.

The gold interconnect has a width of 5 μm and a thickness of 70 nm, while the different channels are approximately 15 μm apart from each other. The encapsulation layer measures approximately 120 μm in width and 2 μm in thickness. The serpentine design of each channel allows the device to be stretchable.

In addition to the electrodes and interconnects, another key component in designing flexible and stretchable neural probes is the method for their insertion into soft tissues. The more flexible and softer the device is, it is more difficult to insert the device into the brain tissue. Various methods have been developed and used to insert flexible devices into soft tissues[18,28–30]. In this thesis, a thin metal wire assists in the insertion of the flexible device for both designs by making a guide hole at the tip of the device. The thin metal probe has a sharp, thinner tip at one end, and this end, with a smaller radius than its body's radius, guides the device into the tissue. The guide hole at the device's tip needs to be slightly smaller than the metal wire body. This way, the wire would not be able to penetrate all the way through the hole when the wire is placed on top of the device and pushed into the tissue. Consequently, the wire pulls the entire flexible device inside the tissue with it. The size of the hole for implantation can differ depending on the choice of wire size. The first device design has a guide hole with a diameter of around 40 μm, while the second device design has a guide hole with a diameter size of 70 μm. The boundary of this guide hole is mechanically reinforced with a layer of gold to prevent the hole from tearing when the wire is inserted, as depicted in Fig. 1d and Fig. 2b.

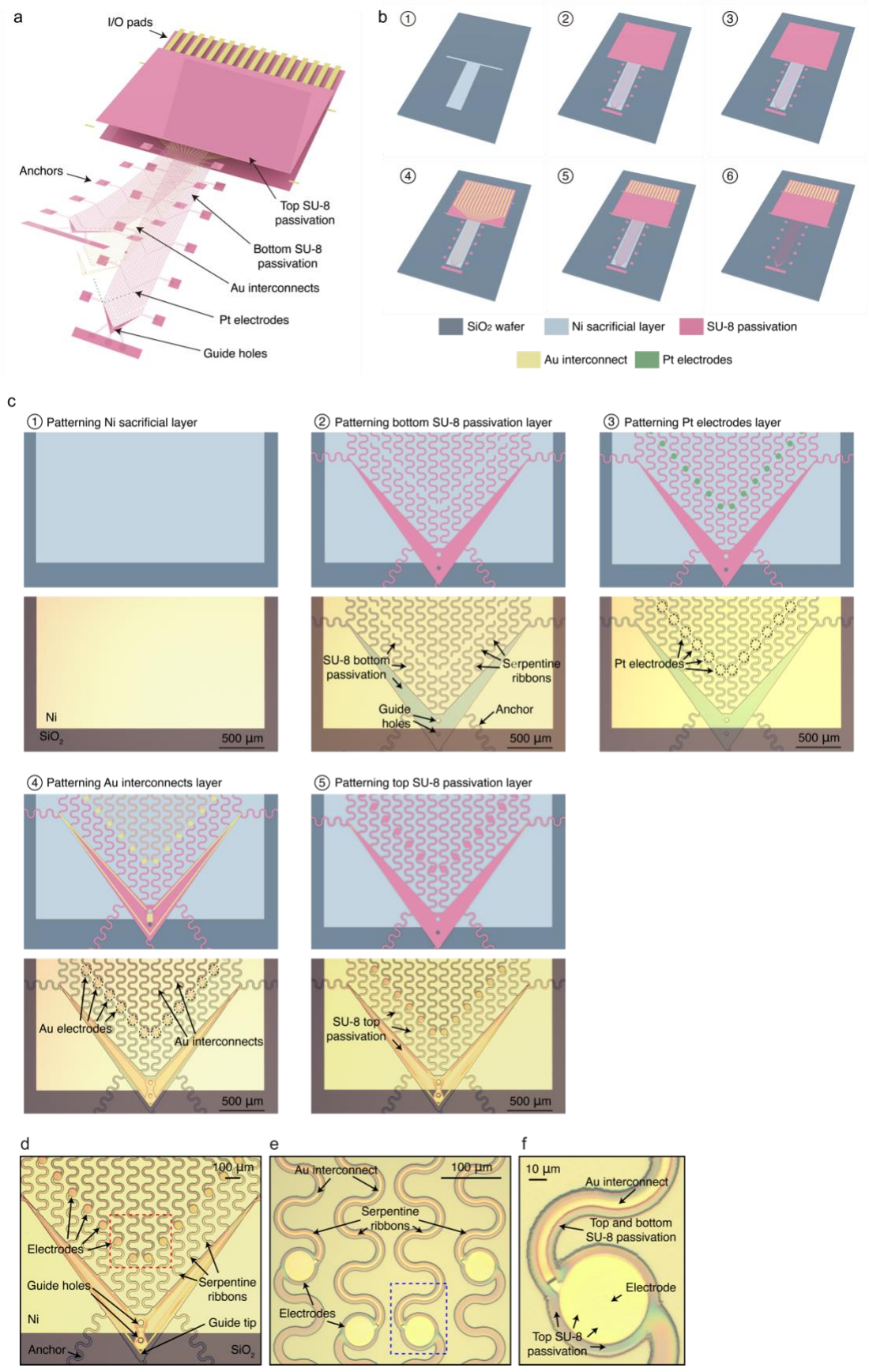
a
I/O pads
Anchors
Top SU-8 passivation
Bottom SU-8 passivation
Au interconnects
Pt electrodes
Guide holes
b
① ② ③ ④ ⑤ ⑥
SiO2 wafer
Ni sacrificial layer
SU-8 passivation
Au interconnect
Pt electrodes
c
① Patterning Ni sacrificial layer
② Patterning bottom SU-8 passivation layer
③ Patterning Pt electrodes layer
Ni
SiO2
500 μm
SU-8 bottom passivation
Serpentine ribbons
Guide holes
Anchor
Pt electrodes
④ Patterning Au interconnects layer
⑤ Patterning top SU-8 passivation layer
Au electrodes
Au interconnects
SU-8 top passivation
d
100 μm
Electrodes
Guide holes
Serpentine ribbons
Ni
Guide tip
Anchor
SiO2
e
Au interconnect
100 μm
Serpentine ribbons
Electrodes
f
10 μm
Au interconnect
Top and bottom SU-8 passivation
Electrode
Top SU-8 passivation

Figure 1 Fabrication procedure for a thin-film flexible electronics device with individual serpentine interconnects. **a** Layer-by-layer schematics of the thin-film electronics device designed with serpentine interconnects, each ribbon containing a single channel. The top and bottom passivation layers are made of SU-8 and the Au interconnect layer is encapsulated between the passivation layers. The electrode sites are coated with an additional Pt layer. **b** Schematics showing the process for the fabrication of thin-film electronics device. The Pt layer is fabricated below the Au layer so that the opening of the electrode faces the wafer. In the final step, the Ni sacrificial layer is removed using Ni etchant, which allows the parts of the device fabricated on top of the Ni layer to be released from the SiO_2 wafer. **c** Schematic and microscope images illustrating each fabricated layer of the thin-film electronics device. The Ni layer, which is first fabricated on top of a clean wafer, will be used as a sacrificial layer. The Bottom SU-8, Pt, Au, and top SU-8 layers are patterned using photolithography sequentially. **d** Image of the tip part of the device after all fabrication steps completed. **e** Close-up image of the red-box region from Fig. 1d. Each serpentine-shaped ribbon is 12 μm-wide, and the Au interconnect is 5 μm-wide. **f** Close-up image of the blue-box region from Fig. 1e. The Pt electrode has a radius of 25 μm.

Chapter 3

3. Fabrication of Thin-film Flexible Electronics

The fabrication experiments were conducted in Harvard Center for Nanoscale Systems (CNS) cleanroom facility.

3.1 Device Fabrication Process

The device fabrication begins with the wafer cleaning. A 3-inch thermal oxide silicon wafer (2005, University wafer) was rinsed with acetone, isopropyl alcohol (IPA), deionized (DI) water, and was blow dried. Then it was treated with O_2 plasma at 100 W, 40 sccm O_2 for 5 minutes. The first step was patterning nickel (Ni) sacrificial layer. To pattern the Ni layer, a photoresist (PR) layer was fabricated. HDMS was spin-coated on the wafer at 3,000 rpm/s for 30 seconds to promote better adhesion of the following layer. As the second PR layer, LOR3A was spin-coated on the wafer at 3,000 rpm/s for 30 seconds and hard-baked at 180 °C for 3 minutes. Lastly, the third PR layer, S1805 was spin-coated on the wafer at 3,000 rpm/s for 30 seconds and hard-baked at 115 °C for 1 minute. Then the photoresists were exposed with 40 mJ/cm2 h-line UV light and developed with CD-26 for 1 minute. The wafer was then rinsed with IPA and DI water and blown dry. After the PR layers were patterned, Ni was deposited using thermal evaporation physical vapor deposition on the wafer (Sharon) to 100 nm thickness and lifted off in Remover PG solution for 3 hours. The wafer was then rinsed with IPA, DI water and blow dried.

The second step was fabricating the bottom SU-8 passivation layer. SU-8 2002 was spin-coated on the wafer at 3,000 rpm/s for 30 seconds and pre-baked at 60 °C for 1 min, then 95°C for 1 minute. SU-8 was then exposed with UV light at dose of 80 mJ/cm^2, then post-baked at 60 °C for 1 minute, 95 °C for 2 minutes. Then SU-8 was developed in SU-8 developer for 2 minutes using a shaker, and rinsed with IPA, water, and blow dried. SU-8 was then hard-baked at 180 °C for 1 hour with gradually increasing and decreasing temperature profiles. The first panel of Figure 2c shows the wafer with Ni and bottom SU-8 fabrication finished. The bright-yellow background is the Ni sacrificial layer, and the darker gray pattern is the bottom SU-8 layer on top of the Ni layer.

The third step was the Au interconnect layer fabrication. The fabrication procedure for patterning PR into Au pattern was identical to the method for Ni pattern PR fabrication. The second panel of Fig. 2c shows the PR pattern of the Au layer. After the PR was successfully patterned, metal layer was deposited using electron-beam physical vapor deposition (Denton). Before and after depositing 70 nm-thick Au layer, 5 nm of chromium (Cr) was deposited to act as the adhesion layer. After deposition, the pattern was lifted off in Remover PG for 6 hours. The third panel of Fig. 2c shows the device after the Cr/Au/Cr deposition and lift-off process.

The fourth step was fabrication of the platinum (Pt) layer. Also identical to patterning Ni or Au PR patterns, the PR for Pt pattern was fabricated first, as can be seen in the fourth panel of Fig. 2c. Then, identical to the Au layer deposition, a 5 nm of Cr adhesion layer and 30 nm of Pt layer was deposited on the gold layer by electron-beam physical vapor deposition. Next, the PR was lifted off in Remover PG for 2 hours and the fifth panel of Fig. 2c is the result.

The last step was fabrication of the top SU-8 passivation layer, which was identical to the bottom SU-8-layer fabrication process. The sixth panel of Fig. 2c is how the finished device looks like. The thickness of the device was around 4 μm in total.

For inverted devices, which have the electrode opening facing towards the wafer, the fabrication procedure is a little altered from the procedure explained above. For this inverted pattern, Pt electrode layer is

fabricated first, right after the Ni sacrificial layer fabrication. Then, the bottom SU-8 layer is fabricated and then the Au interconnect layer is fabricated. The major difference for this Au layer fabrication is that this layer needs to be connected in the patterns on top of the Pt pattern existing on top of the Ni layer and in the other Au patterns existing on top of the around 800 nm-thick bottom SU-8 layer. To achieve this, sputter deposition instead of electron-beam physical vapor deposition process needs to be used. Sputtering allows for deposition of Au from an angle with respect to the vertical axis, and thus can also coat the sidewall of the SU-8 layer if the sputtering is done while the wafer is rotating. After Au layer deposition and lift-off, the top SU-8 passivation layer is fabricated, and the rest of the process is identical.

The patterns developed and lift-offed have no defect and have clean, straight boundaries. After the device being fabricated without defects and have good adhesion between the layers and good alignment, the device undergoes post-fabrication device processes and electrical characterization in saline solution.

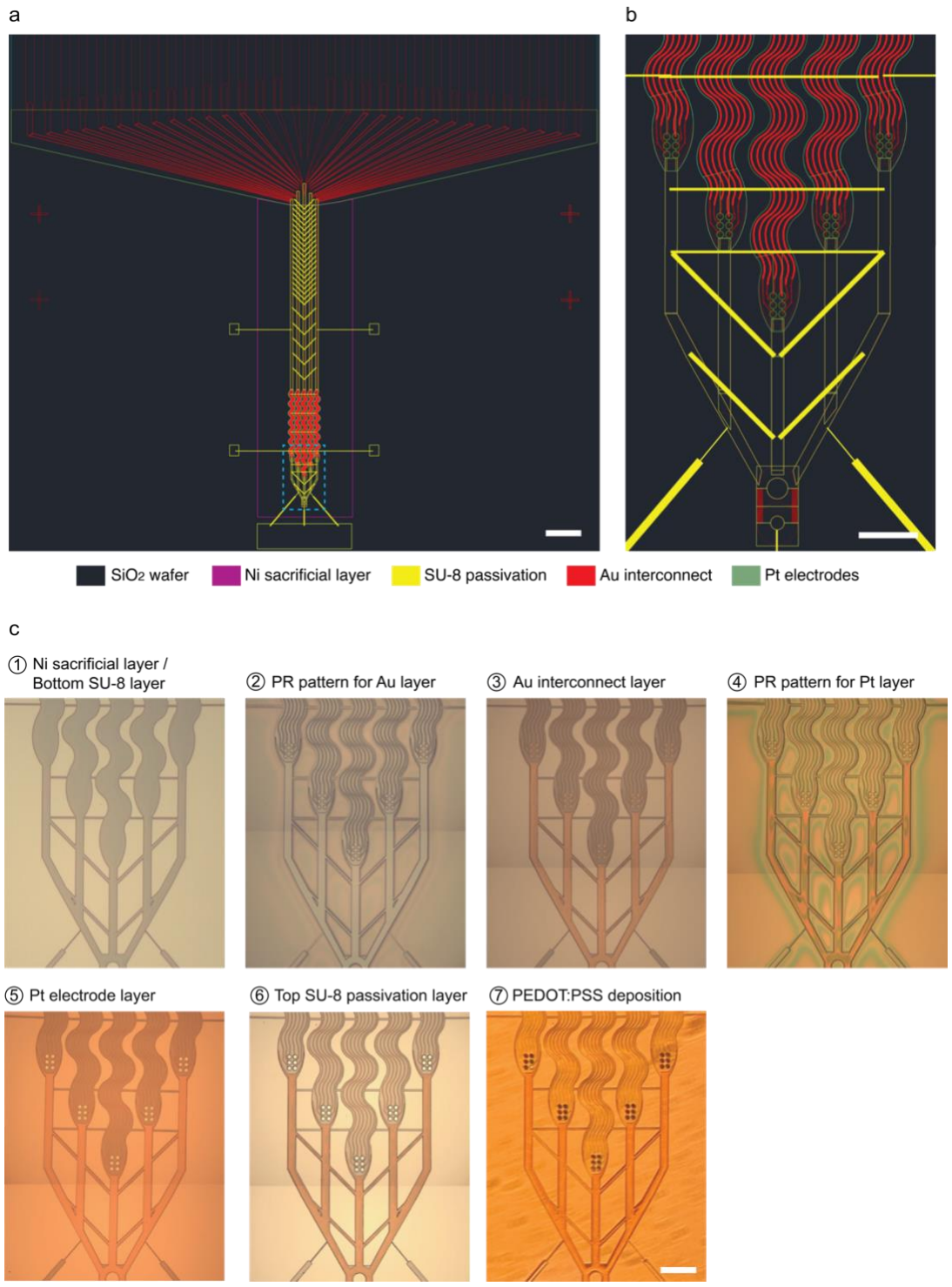

Figure 2 Fabrication procedure for thin-film flexible electronics device with tetrode-like electrodes. **a** The design of the thin-film electronics device with tetrode-like electrodes. There are five tetrode-like electrode sets, each set having six electrodes, each 30 μm apart from the closest electrodes. In total, there are 30 channels for recording. Each tetrode-like electrode set is bundled into a single serpentine-shaped ribbon. The total width of the device implanted into the brain is around 1 mm. Scale bar: 1 mm. **b** A close-up image of the blue-box region from Fig. 3a. There exist two guide holes for the metal guide wire at the tip of the

device. Scale bar: 200 μm. **c** Microscope images each showing the fabrication steps for the thin-film electronics device. Similar to the previous device design, the Ni sacrificial layer and the bottom SU-8 layer are fabricated. For this device, the Pt electrode layer is fabricated on top of the Au interconnect layer, making the electrode face the further side from the wafer. For Au and Pt layers, a photoresist (PR) layer is first made and patterned using photolithography and then the metal is deposited on top. Then, the PR layer is removed, leaving the metals having the inverted pattern. After the top SU-8 layer fabrication, a conductive polymer, poly (3, 4-ethylenedioxythiophene):poly(styrene sulfonate) (PEDOT:PSS), is electrochemically deposited on top of the electrodes to decrease the interfacial impedance. Scale bar: 200 μm.

3.2 Post-fabrication Device Processing

After fabrication of all the layers of the device, the 3-inch wafer was diced into several smaller pieces since a single wafer have 9 to 12 identical devices to increase the fabrication throughput. For dicing, the wafer was spin-coated with PR S1813 at 4,000 rpm/s for 1 minute to protect the device during dicing. Then the wafer was cut using a dicing saw and the PR coating was removed with PG remover for 5 minutes, rinsed with IPA and DI water and blow dried.

After having one device for each wafer piece, a flexible flat cable (FFC, Molex) was attached onto the Au I/O pads using a flip-chip bonder (Finetech), with the maximum temperature of 180 °C. The connection area was covered with silicone elastomer (World Precision Instruments) to stabilize the connection mechanically and chemically.

After the silicone elastomer was fully set, PEDOT:PSS was electrochemically deposited onto the electrodes to check the electrical connectivity of the channels and decrease the interfacial impedance of the electrodes. The seventh panel of Fig. 2c shows the device after PEDOT:PSS deposition.

After the device was confirmed that it has good electrical connection and passivation as we intended, the devices were released and prepared for implantation. The device was submerged under Ni etchant (TFB, Transene Company) for 3-4 hours at 30 °C. The device was only submerged to the level of all the electrodes being under the etchant, so the I/O pads of FFC would not be in contact with the etchant. After entire removal of the Ni layer, the device was released and washed with caution with DI water.

3.3 Device characterization

After the devices were finished fabricating and flip-chip-bonding to a FFC cable, the impedance values were measured after releasing the devices. The in vitro impedance measurement was conducted in saline solution with a platinum reference probe also submerged into the identical saline solution bath. The impedance measurement system was conducted using CerePlex Direct recording system (Blackrock Microsystems). Fig 3a shows the impedance measurement results from 10 different devices each having 30 channels. The devices are from 3 different fabrication batches, and all are in acceptable range of impedances values around 300 to 1200 kΩs.

Chapter 4

4. In-vivo Implantation of Flexible Electronics

4.1 Implantation of Flexible Electronics

In order to demonstrate the device implantation method and the signal recording capability of the device, the device was implanted in hippocampus CA1 region (M/L: -1.4, A/P: -1.8, D/V: -1.5)[31] in 3 mice. Mice were C57/BL6 adult males at 8 weeks of age (Charles River Laboratories). Mice were kept on a regular 12 hour-12hour light-dark cycle with temperature and humidity-controlled facility. Experimental procedures were approved by the Institutional Animal Care and Use Committee (IACUC) of Harvard under the animal protocol 19-03-348-1 and followed guidelines from the National Institutes of Health throughout all the surgeries and procedures. No surgery or experiment had been performed on the animals prior to the surgery. The animal was anesthetized with 3% isoflurane and kept under anesthesia with 1% isoflurane during the whole surgery.

For implantation, the skin on top of the animal's head was removed with surgical scissors. This removal of skin needs to be much larger than the size of the implantation area, which is to create enough surface area in the skull for the device and ground electrodes to be stably mounted for extended period of time. After the skull was exposed, the implantation site was determined using the coordinates of the CA1 region. Then, a small cranial opening, with a size of slightly larger than the device (2 mm by 2 mm) was made using a hand-held drill. The dura and pia mater were first removed, and the thin-film electronics device was slowly inserted using the tungsten guide wire (A-M SYSTMES, 797550) until all the electrodes were inserted and reached the exact coordinates. The tungsten wire served as implantation shuttle and was withdrawn when

the device was inserted in the brain. Figure 3b shows various types of devices being successfully inserted using the tungsten guide wire. The guide wire was first aligned to fit perfectly at the guide hole located at the tip of the device. Then, sterile saline solution was applied near the device so that the device would experience less stress during the insertion process. As the guide wire was inserted inside the tissue, the device was also moved closer to the insertion location so that no additional stress would be given to the device. A 500 um-thick stainless-steel wire (A-M SYSTMES, 794100) was inserted on the opposite hemisphere to be used as the ground electrode. The device and the ground electrode were carefully fixed in place and the surgery area was covered and sealed with dental cement.

Including the surgery day and up to 96 hours post-surgery, postoperative care was given, and the animals' activity, surgery region inflammation, and pain level were closely monitored at least twice a day. Analgesics were given up to 48 hours after surgery, using Carprofen (20 mg/kg) and extended-release buprenorphine (3.25 mg/kg).

After implantation and signal recording, the brain was harvested to confirm the actual location after implantation. The mice were anesthetized via 3% isoflurane inhalation and sodium pentobarbital injection (40-50 mg/kg) and performed transcardiac perfusion using 50 mL of phosphate buffered saline (PBS), and then 50 mL of 4% paraformaldehyde (PFA) in PBS solution. After decapitation, the head was placed inside the 4% PFA solution for 24 hours at 4 ℃. Then, the brain was harvested from the head by removing the skin and skull and submerged in 15% sucrose in PBS solution for 12 hours at 4 ℃, and 30% sucrose in PBS solution for 24 hours at 4 ℃. This procedure allows for the brain tissue to be less fragile when handling and better quality-sections. The brain tissue was then placed inside a tissue mold with O.C.T. solution (Tissue-Tek). The solution containing the brain was frozen at -20 ℃ and cryosectioned into 30 μm-thick slices using cryostat. The sections were then observed one-by-one under a bright-field microscope to confirm the devices were successfully implanted and stayed in place inside the brain tissue. Figure 3c shows the frozen brain tissue inside OCT solution, mounted on the cryostat to cut thin brain sections. Figure 3d is an example of a bright-field image of a brain tissue section that contains multiple electrodes from the device

implanted. The white arrows indicate the 50 μm-diameter electrodes, and the serpentine-shaped interconnects are also visible, connected to the electrodes.

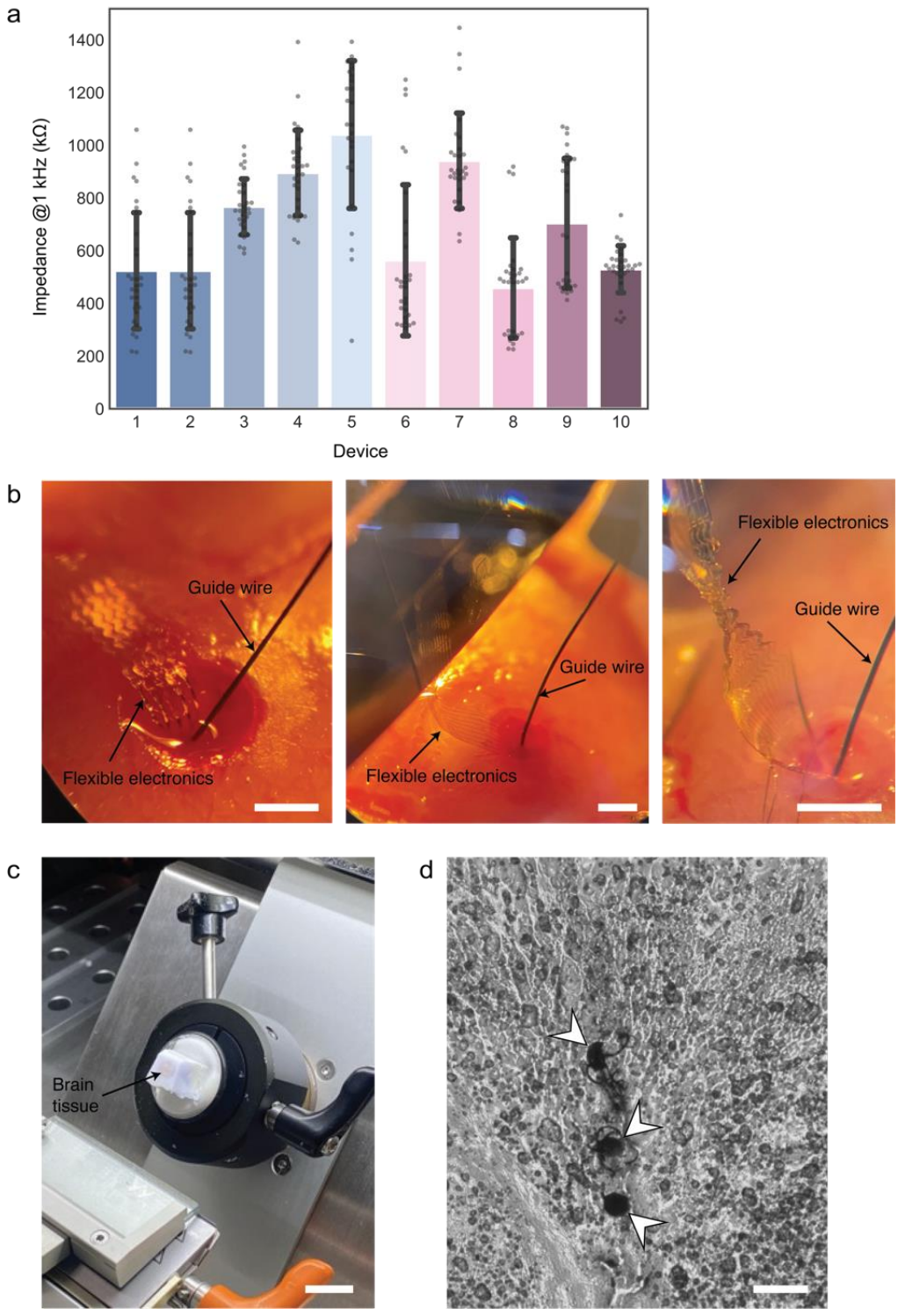

Figure 3 Characterization and in vivo implantation of thin-film electronics with tetrode-like electrodes in mouse brains. **a** Impedance values of the thin-film electronics with tetrode-like electrodes at 1 kHz measured from 10 different devices in several different fabrication batches. The bar graphs show the average values, and the error bars describe the standard deviation values. **b** Implantation of the fabricated and post-processed devices in mouse brains via stereotaxic brain surgery. The metal guide wire is positioned on top of the guide hole at the tip of the device, and the guide wire is inserted inside the brain, pulling the thin-film electronics device into the brain. This implantation method can be used for several different designs of devices. Scale bars: 1 mm. **c** Cryosection process of brain harvested after device implantation. A cryostat is used to section the brain tissue into thin slides. Scale bar: 5 cm. **d** A bright-field image of a brain tissue section with the serpentine device implanted. The three arrows show the electrodes. The Au interconnects connected to the electrodes can also be seen in the image as the dark lines in between the electrodes. Scale bar: 100 μm.

4.2 In-vivo Neural Signal Measurements

After the devices were implanted on mouse brains, the neural signals were measured from week 1 post-surgery. After the first week, the recording was done once every 1 week until week 3 after surgery. The neural signals of the mice were recorded using the CerePlex Direct recording system (Blackrock Microsystems). The setup was placed on an optical table to remove any external vibration and surrounded by a Faraday cage to prevent external electric field to interfere with our recording. The recording was conducted with all the lights off and the mouse was kept under anesthesia using 1% isoflurane inhalation during the recording sessions.

The sampling rate was 10 kHz and the device having tetrode-like electrodes was used for signal recording. The recorded raw data passed through a voltage amplifier in the headstage and then saved. The analysis was conducted after all the recording sessions were finished.

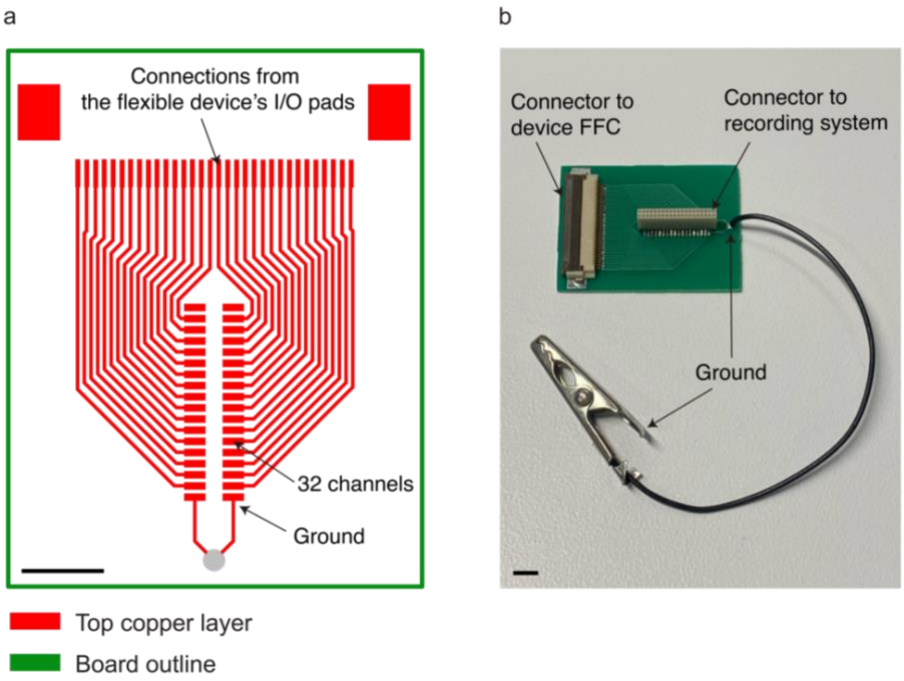

Figure 4 Custom PCB design for connection of the thin-film flexible device to the recording system. **a** The PCB design for connecting two connectors, each establishing a connection from the FFC attached to the thin-film device to the omnetics connector attached to the signal acquisition recording system headstage. There are 32 number of recording channels and two channels for ground. **b** The actual image of the custom-designed PCB. The connector on the left is an FFC connector which would receive signals acquired from the thin-film electronics device. The connector on the right will send the signals to the CerePlex Direct recording system which will then be amplified and processed for data analysis. The ground is connected to an alligator clip which is connected to the ground electrode implanted in the brain. Scale bar: 5 mm.

The data analysis pipeline is as follows. First, the raw recording data, or traces, obtained from multiple recording sessions across multiple weeks are loaded and concatenated into a single file. Next, the traces are associated with appropriate probe channel number and its geometry. The traces are then preprocessed before sorting process, using 300-3000 Hz bandpass filter and common median referencing (CMR)[32]. This removed most of the background noise and common-mode noise. The left panel of Figure 5a shows the preprocessed recording traces after bandpass filtering and CMR. Each trace was recorded from different electrodes and each trace are unique, which implies that they were not shorted with other channels. Each tetrode-like electrode sets were composed of six electrodes, and thus six electrodes acquired similar neural signal patterns at similar point of time. The right panel of Figure 5a is a close-up trace from the left panel, showing a more detailed traces from each channel.

The preprocessed data was then spike sorted using the MountainSort4 algorithm[33] using the SpikeInterface package[34]. Then, the waveforms were extracted from the sorting result and real neural signals were curated by referring to various data: the pre-processed traces, channel heatmap of signals, templates, interspike interval distributions, spike autocorrelograms, and 2D mapping of waveforms using uniform manifold approximation and projection (UMAP)[35]. Figure 5 shows some of the spike sorting results obtained via the analysis pipeline. Figure 5b is an example of templates of single-unit waveforms obtained using the recording data from week 1 to week 3. Templates are the average waveforms of each single unit. In Figure 5c, the templates for each week are shown and the amplitude of the templates tend to increase and noise level tend to decrease in later recordings. Using the waveforms obtained from the 6 tetrode-like electrode set channels having the highest-amplitude, each spiking event's waveform was projected into 2D embedding space of UMAP. This shows the stability of each single-unit recordings. The first week's recording has a smaller number of spiking events due to not enough recovery time from the surgical damage near the electrodes. However, the distribution of the mappings from different week's recordings are stable across different times, showing that the thin-film flexible electronics device can record neural signals from the same neurons across different weeks.

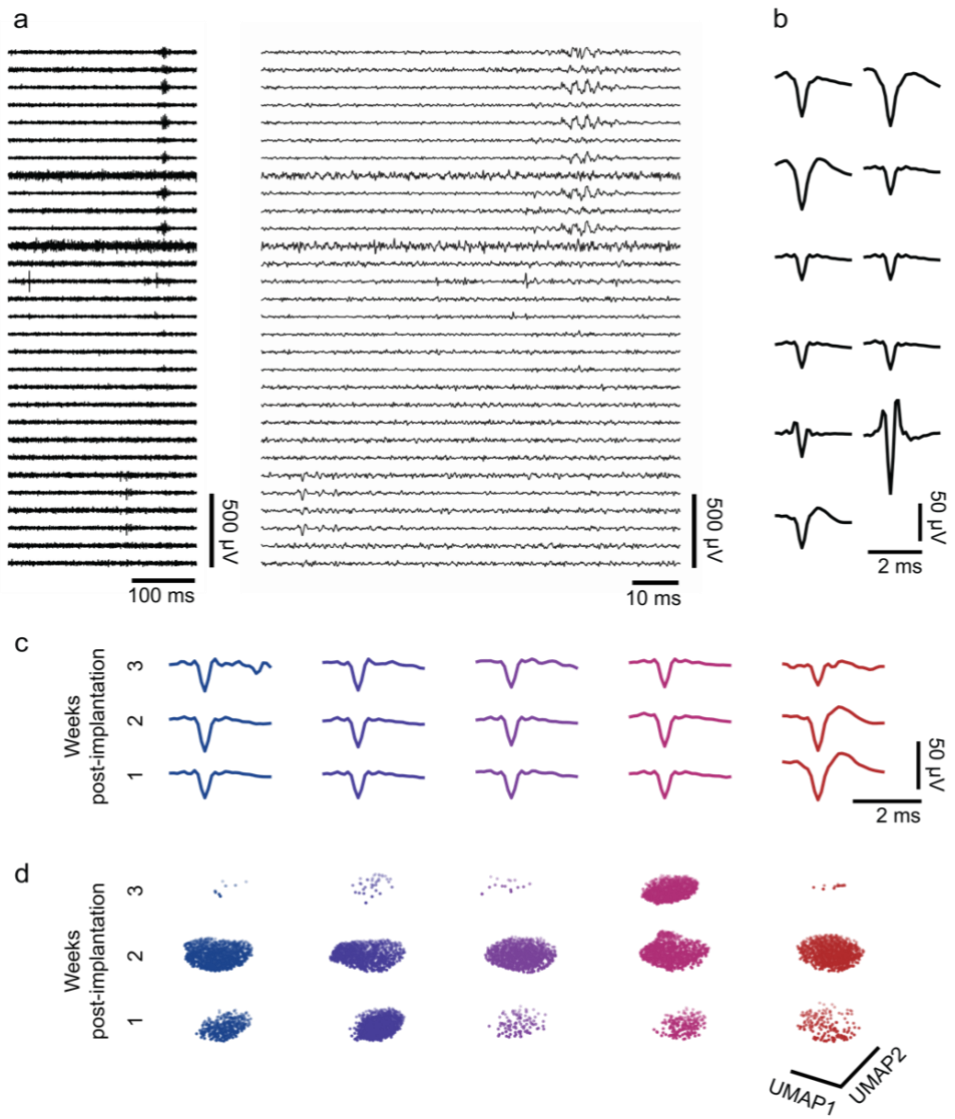

Figure 5 Neural signal recording data from mouse brains collected using thin-film electronics with tetrode-like electrodes. **a** Left: a representative voltage trace data after bandpass filtering (300-3000 Hz). The data was recorded 2 weeks after implantation. Right: a close-up voltage trace data from the left panel. **b** Templates, or the average single-unit waveforms, detected from the three weekly recording sessions from a mouse after implantation. The entire session, recorded at one, two- and three-weeks post-implantation, is 45 minutes long. **c** Templates, or the average single-unit waveforms each from one, two- and three-weeks post-implantation. **d** Clusters of the single-unit waveforms detected in Fig. 5c placed in UMAP space. Each cluster is from one, two- and three-weeks post-implantation. The same column in Fig. 5c and 5d represents the same unit detected.

Chapter 5

5. Conclusion

This thesis presented designs for thin-film flexible and stretchable devices capable of acquiring single-unit neural signals and analyzed *in vivo* neural signal recording data, observing weekly changes in the measured data. The recent advances in materials, design, and computation algorithms in thin-film electronic devices now enable the recording of *in vivo* neural signals for periods exceeding 6 months and even years. Such long-term stable flexible thin-film electronics devices hold promise for various applications and purposes. The design principles and fabrication methods outlined in this thesis pave the way for endless types of designs tailored to specific applications and goals.

Given that the research area of developing tools for recording brain signals and analyzing them is highly multidisciplinary, achieving future milestones requires advancements in various fields. Some future milestones include developing sensors that can be spatially scaled up to multiple brain regions or record from multi-thousands of neurons across the whole organ, with high throughput for fabrication. New materials or fabrication methods could facilitate progress toward these milestones. Sensors and stimulators operating in multimodal fashion, such as combining electrical recording with selective optical stimulation and chemical treatments that can have long-term stability over multiple years would revolutionize the field. In terms of computation, on-chip processing for real-time and adaptive decision-making will allow for personalized medical treatments using long-term stable brain interface. Additionally, devices capable of achieving stable recording capability in growing brains or tissues will open new ways of studying developmental processes or diseases.

Chapter 6

6. Bibliographic References

1. Donoghue, J. P. Bridging the Brain to the World: A Perspective on Neural Interface Systems. *Neuron* **60**, 511–521 (2008).
2. Willett, F. R., Avansino, D. T., Hochberg, L. R., Henderson, J. M. & Shenoy, K. V. High-performance brain-to-text communication via handwriting. *Nature* **593**, 249–254 (2021).
3. Hochberg, L. R. *et al.* Reach and grasp by people with tetraplegia using a neurally controlled robotic arm. *Nature* **485**, 372–375 (2012).
4. Raspopovic, S. *et al.* Restoring Natural Sensory Feedback in Real-Time Bidirectional Hand Prostheses. *Sci. Transl. Med.* **6**, 222ra19-222ra19 (2014).
5. Lazarou, I., Nikolopoulos, S., Petrantonakis, P. C., Kompatsiaris, I. & Tsolaki, M. EEG-based brain–computer interfaces for communication and rehabilitation of people with motor impairment: a novel approach of the 21 st Century. *Front. Hum. Neurosci.* **12**, 14 (2018).
6. Machado, Sergio *et al.* EEG-based Brain-Computer Interfaces: An Overview of Basic Concepts and Clinical Applications in Neurorehabilitation. *Rev. Neurosci.* **21**, 451–468 (2010).
7. Schalk, G. & Leuthardt, E. C. Brain-Computer Interfaces Using Electrocorticographic Signals. *IEEE Rev. Biomed. Eng.* **4**, 140–154 (2011).
8. Miller, K. J., Hermes, D. & Staff, N. P. The current state of electrocorticography-based brain–computer interfaces. *Neurosurg. Focus* **49**, E2 (2020).

9. Li, W., Rodger, D., Menon, P. & Tai, Y.-C. Corrosion Behavior of Parylene-Metal-Parylene Thin Films in Saline. *ECS Trans.* **11**, 1 (2008).
10. Wang, A. *et al.* Stability of and inflammatory response to silicon coated with a fluoroalkyl self-assembled monolayer in the central nervous system. *J. Biomed. Mater. Res. A* **81A**, 363–372 (2007).
11. Maynard, E. M., Nordhausen, C. T. & Normann, R. A. The Utah Intracortical Electrode Array: A recording structure for potential brain-computer interfaces. *Electroencephalogr. Clin. Neurophysiol.* **102**, 228–239 (1997).
12. R. J. Vetter, J. C. Williams, J. F. Hetke, E. A. Nunamaker, & D. R. Kipke. Chronic neural recording using silicon-substrate microelectrode arrays implanted in cerebral cortex. *IEEE Trans. Biomed. Eng.* **51**, 896–904 (2004).
13. Budday, S. *et al.* Mechanical properties of gray and white matter brain tissue by indentation. *J. Mech. Behav. Biomed. Mater.* **46**, 318–330 (2015).
14. Viventi, J. *et al.* Flexible, foldable, actively multiplexed, high-density electrode array for mapping brain activity in vivo. *Nat. Neurosci.* **14**, 1599–1605 (2011).
15. Chung, J. E. *et al.* High-Density, Long-Lasting, and Multi-region Electrophysiological Recordings Using Polymer Electrode Arrays. *Neuron* **101**, 21-31.e5 (2019).
16. Luan, L. *et al.* Ultraflexible nanoelectronic probes form reliable, glial scar–free neural integration. *Sci. Adv.* (2017) doi:10.1126/sciadv.1601966.
17. Fu, T.-M. *et al.* Stable long-term chronic brain mapping at the single-neuron level. *Nat. Methods* **13**, 875–882 (2016).
18. Zhao, S. *et al.* Tracking neural activity from the same cells during the entire adult life of mice. *Nat. Neurosci.* **26**, 696–710 (2023).
19. Kato, Y., Furukawa, S., Samejima, K., Hironaka, N. & Kashino, M. Photosensitive-polyimide based method for fabricating various neural electrode architectures. *Front. Neuroengineering* **5**, (2012).
20. Le Floch, P. *et al.* Fundamental Limits to the Electrochemical Impedance Stability of Dielectric Elastomers in Bioelectronics. *Nano Lett.* **20**, 224–233 (2020).

21. Le Floch, P. *et al.* 3D spatiotemporally scalable in vivo neural probes based on fluorinated elastomers. *Nat. Nanotechnol.* 1–11 (2023) doi:10.1038/s41565-023-01545-6.

22. Liu, J. *et al.* Fully stretchable active-matrix organic light-emitting electrochemical cell array. *Nat. Commun.* **11**, 3362 (2020).

23. Dauzon, E. *et al.* Conducting and Stretchable PEDOT:PSS Electrodes: Role of Additives on Self-Assembly, Morphology, and Transport. *ACS Appl. Mater. Interfaces* **11**, 17570–17582 (2019).

24. Szostak, K. M., Grand, L. & Constandinou, T. G. Neural Interfaces for Intracortical Recording: Requirements, Fabrication Methods, and Characteristics. *Front. Neurosci.* **11**, 665 (2017).

25. Yang, X. *et al.* Bioinspired neuron-like electronics. *Nat. Mater.* **18**, 510–517 (2019).

26. Yan, C. *et al.* Automated and Accurate Detection of Soma Location and Surface Morphology in Large-Scale 3D Neuron Images. *PLOS ONE* **8**, e62579 (2013).

27. Widlund, T., Yang, S., Hsu, Y.-Y. & Lu, N. Stretchability and compliance of freestanding serpentine-shaped ribbons. *Int. J. Solids Struct.* **51**, 4026–4037 (2014).

28. Zhao, Z. *et al.* Parallel, minimally-invasive implantation of ultra-flexible neural electrode arrays. *J. Neural Eng.* **16**, 035001 (2019).

29. Novel diamond shuttle to deliver flexible neural probe with reduced tissue compression | Microsystems & Nanoengineering. https://www.nature.com/articles/s41378-020-0149-z.

30. Du, Z. J. *et al.* Ultrasoft microwire neural electrodes improve chronic tissue integration. *Acta Biomater.* **53**, 46–58 (2017).

31. Paxinos, G. & Keith B.J., F. *The Mouse Brain in Stereotaxic Coordinates: Hard Cover Edition*. (2001).

32. Rolston, J. D., Gross, R. E. & Potter, S. M. Common median referencing for improved action potential detection with multielectrode arrays. *Annu. Int. Conf. IEEE Eng. Med. Biol. Soc. IEEE Eng. Med. Biol. Soc. Annu. Int. Conf.* **2009**, 1604–1607 (2009).

33. Chung, J. E. *et al.* A Fully Automated Approach to Spike Sorting. *Neuron* **95**, 1381-1394.e6 (2017).

34. Buccino, A. P. *et al.* SpikeInterface, a unified framework for spike sorting. *eLife* **9**, e61834 (2020).

35. McInnes, L., Healy, J. & Melville, J. UMAP: Uniform Manifold Approximation and Projection for Dimension Reduction. Preprint at https://doi.org/10.48550/arXiv.1802.03426 (2020).